Algal Research 79 (2024) 103434

Contents lists available at ScienceDirect

Algal Research

journal homepage: www.elsevier.com/locate/algal

Application of passive vortex generators to enhance vertical mixing in an open raceway pond

Chen Shen *, David S. Dandy

Department of Chemical and Biological Engineering, College of Engineering, Colorado State University, Fort Collins, CO, United States of America

ARTICLE INFO

Keywords:
LES
Raceway pond
Swirling
Vortex generator
L/D effect
CFD

ABSTRACT

A novel use of vortex generators in a raceway pond is described here, with the flow field quantitatively simulated using computational fluid dynamics using the large eddy simulation turbulence model. Persistence lengths of the swirling motion generated by the vortex generators indicate that significant vertical mixing can be achieved by placing vortex generators in the straight section opposite the paddle wheel, downstream of the first hairpin bend. Relatively simple vortex generators are capable of creating stronger swirling motions that persist for a longer distance than those created by the paddle wheel. For optimal performance, vortex generators are positioned side by side but in opposite directions, and their diameters should be equal to or slightly less than the desired liquid depth. The optimal length of a 0.18 m diameter vortex generator in a 0.2 m deep pond was determined to be 0.3 m. Furthermore, it has been demonstrated that a longer persistence length is achieved by inducing a swirling motion with its rotational axis parallel to the primary flow direction.

1. Introduction

Due to the depletion of fossil fuels, biofuel production has drawn significant attention as a substitute for fossil fuels. Microalgae utilize solar energy and absorb CO_2 to generate mid-products such as lipids, which can be converted to biofuels. As a result, microalgae-based biofuel is a promising substitute for fossil fuel as it has an extremely fast growth rate, can make use of nutrients from wastewater, yields high lipid carbohydrate content, does not compete with food crops for arable land, can produce high-value by-product chemicals and reduce global warming [1,2].

Microalgae can be cultivated in closed photobioreactors such as tubular or flat panel reactors or outdoor open reactors [3–5]. Raceway ponds are one of the most popular and preferable outdoor cultivation systems as they are simple to construct and scale up, require small capital investment, are easy to maintain, and require low energy inputs to operate [6–8]. The ponds consist of an oval-shaped channel with a divider placed in the center of the straight sections. One or multiple paddle wheels are installed to drive the flow around the track. Subject to the liquid flow motion, the vertical positions of microalgae cells are constantly changing, and the light each cell receives is consequently changing dynamically. It has been reported that microalgae have the potential to yield an improved production rate when the cells are exposed to light sources that frequently change between light and dark, which is known as the light/dark (L/D) effect [9–11]. Other than enhancing the L/D effect, vertical mixing also prevents cell stacking and biofilm formation, improves mass transfer, reduces thermal stratification, and avoids oxygen accumulation [12–14].

Computational fluid dynamics (CFD) simulations have been widely utilized to design and study flows in photobioreactors (PBRs) and open raceway pond systems by solving the Navier-Stock equations and incorporating suitable turbulence models [15–18]. CFD can be used as an effective design tool, accurately describing flow field details prior to construction and experimentation, hence saving significant time and cost. Multiple studies have been conducted to improve the mixing performance of raceway ponds. Voleti investigated the effect of installing delta wings in open raceway pond system [19]. The flow field and turbulence were measured by Acoustic Doppler Velocimetry and Particle Image Velocimetry methods. It was reported that multiple longitudinal streamwise vortices were generated downstream of a delta wing placed in the straight section and were sustained for a distance of up to 3 m. The vertical mixing enhancement was demonstrated by computing and comparing the vertical mixing index of the raceway with and without a delta wing. A novel mixing baffle for open raceway ponds has been proposed by Zongbo et al. [20]. A 24 % decrease of the L/D cycle period and a 22 % increase of the biomass yield were achieved by placing up-

* Corresponding author.
E-mail address: chen.shen@dupont.com (C. Shen).

https://doi.org/10.1016/j.algal.2024.103434
Received 21 September 2023; Received in revised form 10 December 2023; Accepted 13 February 2024
Available online 19 February 2024

down chute baffles in a raceway pond. Qinghua et al. have reported on the influence of the flow field of a raceway pond with flow deflectors and wing baffles [21]. CFD simulations and particle tracking demonstrated that, with the addition of wing baffles, swirling flow was generated, and particles moved more regularly in the light path direction. Additionally, it has been reported that with the wing baffles in place, the dead zone volume decreased by 60.42 %, and the biomass yield increased by 30.11 %. However, the vertical motion generated by chute baffles and wing baffles has axes parallel to the direction of the primary flow. One hypothesis is that if swirling motions can be generated in such a way that the axis is longitudinal, as are the swirling motions generated by bend geometries, the swirling motions will persist for a longer distance.

In this work, a novel design of a vortex generator that can efficiently convert horizontal fluid motion into vertical swirling motion is presented. CFD simulations are carried out with vortex generators placed in the second straight section where the natural vertical motion is predicted to be very low. The vortex generators are studied in a straight channel as well to eliminate the effect of the downstream hairpin bend. An algorithm to determine the persistence length of the generated swirling motion with a given critical velocity is developed. The placement strategy, the optimal diameter D_{opt} for a given liquid depth, as well as the optimal length L_{opt} for a 0.18 m diameter vortex generator in a 0.2 m deep pond, is determined by analysis of CFD simulation results.

2. Material and methods

2.1. The geometry of the vortex generator and the raceway ponds

The vortex generator is composed of a cylindrical outer surface and a propeller-like internal structure, as shown in Fig. 1a. The internal structure consists of 5 propeller-shaped blades that are connected to an axle located in the center of the generator. Based on a nominal pond depth of 0.20 m, the internal diameter of the vortex generator is set to 0.16 m, and the thickness of the outer cylinder is 0.01 m, such that the outer diameter for all the vortex generators studied is 0.18 m. The blades are designed to be parallel to the main flow at the generator inlet for 0.033 m, and then curve gradually to prevent the flow from abruptly changing direction, which might create an excessive wake zone downstream of the blades and deteriorate the ability to generate vortices. The pitch of the vortex blades is given in Fig. 2.

The vortex generator is extruded to different lengths (0.1, 0.15, 0.2, 0.25, 0.3, and 0.4 m) using the same pitch of the blades in order to identify the L_{opt} that creates the strongest vortices that persist the longest distance. The vortex generators are placed in a long raceway pond as well as in a straight channel. The tested raceway pond is designed to be long enough so that most of the swirling motion generated by the 180° bend will dissipate before the flow reaches the generators. In this way, the performance of the generators can be fully quantified in a region where flow is largely horizontal. After analyzing the performance of the generators in unidirectional and counter-directional blade configurations to determine the best orientation, the vortex generators with the six lengths are positioned in a straight channel without the hairpin bends present to eliminate the swirling motion generated by the hairpin bends and simultaneously minimize computational costs. The straight section of the raceway pond modeled here measures 6 m in length and 1 m in width. The thickness of the divider in the raceway is set to 0.04 m. The paddle wheel is located in the middle of the first straight section, and the vortex generators are placed near the center of the second straight section. The separate straight channel is 9 m long, measured from the inlet to the outlet and 0.48 m wide, that is, the width of a straight section in the raceway pond. The paddle is positioned 1 m downstream of the inlet, and the vortex generators are placed 3.0 to 3.4 m downstream of the inlet, depending on generator length. The quiescent water depth is set to be 0.2 m for all cases. To facilitate reader convenience and quick reference, Table 1 provides the model parameters and corresponding figure numbers for each simulated case.

2.2. Mesh generation, solver, and numerical setup

The numerical solution method uses the “interFoam” solver under the openFoam 6.0.0 framework [22]. The residual evaluation is included at the conclusion of each inner pressure correction loop with splitting of operators (PISO) iteration, and the inner pressure corrector loop is configured to terminate when the residual approaches the target residual to improve performance while maintaining stability. The simulations are carried out on a high-performance computer at the National Renewable Energy Laboratory equipped with dual Intel Xeon Gold Skylake 6154 processors (3.0 GHz, 18 cores). An average of 6912 core-hours were used to collect flow time history data for each of the cases.

The computational grid is generated using the ANSYS meshing utility and then converted to the openFoam format. To simulate the rotational motion of the paddle wheel, the fluid domain is meshed separately as a static domain and a rotational domain. The interface between these two domains is coupled by an arbitrary coupled mesh interface (ACMI) boundary condition. The ACMI boundary condition is an extension of the arbitrary mesh interface (AMI) boundary condition that incorporates the local Galerkin projection method to smoothly interpolate non-conforming faces between two adjacent volume meshes [23]. To ensure accuracy and resolve eddies of all scales, fine meshes with an average mesh size of 4,333,000 cells are employed for the simulations.

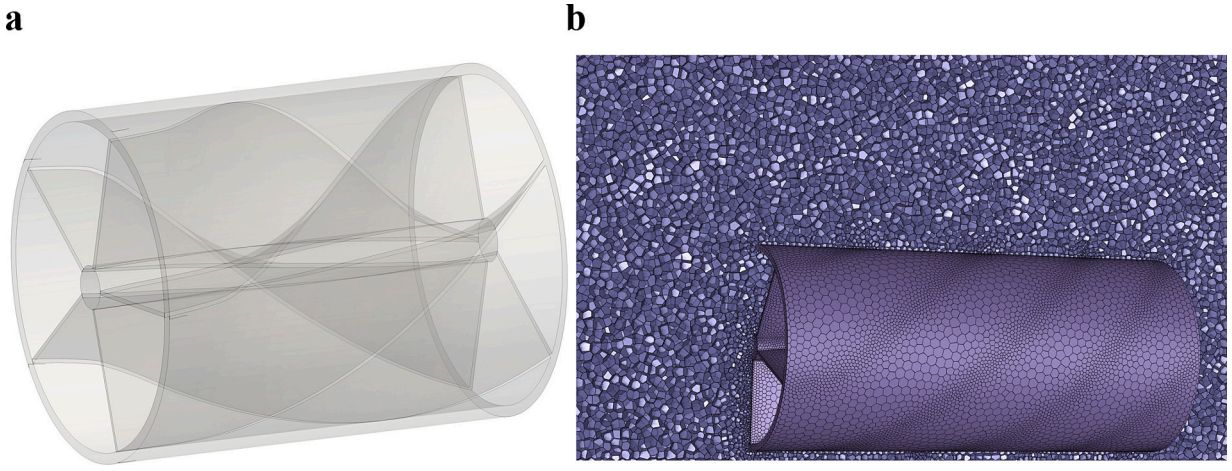

Fig. 1. (a) Geometric design of the vortex generator. (b) A vertical plane showing the mesh of the vortex generator zone generated by ANSYS mosaic meshing algorithm.

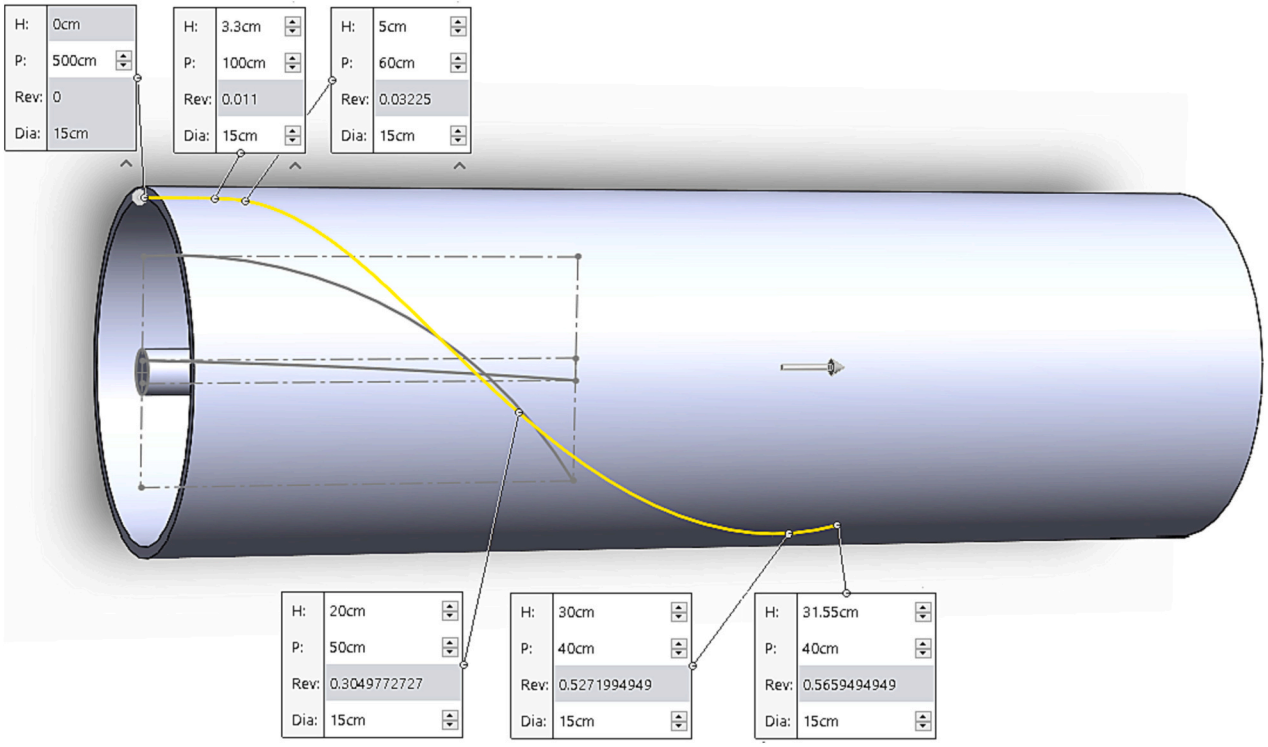

Fig. 2. Solidwork schematic diagram of the vortex generator with the blades' pitch parameters. H: height; P: pitch; Rev.: revolution; Dia: diameter.

Table 1
Summary of simulated cases, including model parameters and the respective figure numbers presenting the results. The persistence lengths are calculated with critical vertical velocity = 0.12 m/s.

Simulation case	Model geometry	Water depth (m)	With vortex generator	Generator deployment configuration	Generator length (m)	Persistence length (m)	Paddle persistence length (m)	Figure
1	Raceway pond	0.20	no	N/A	0.20	N/A	N/A	4.a
2		0.20	yes	Same direction	0.20	N/A	N/A	4.c
3		0.20		Counter direction	0.20	N/A	N/A	4.b; 4.d; 5
4		0.10			0.20	N/A	N/A	6.a
5		0.15			0.20	N/A	N/A	6.b
6		0.25			0.20	N/A	N/A	6.c
7	Straight channel	0.20	yes	Counter direction	0.10	3.90	1.74	7
8					0.15	3.73	1.71	
9					0.20	4.04	1.73	
10					0.25	4.14	1.74	
11					0.30	4.72	1.77	
12					0.40	3.06	1.74	

Due to the intricate geometric design of the vortex generator and the presence of sharp angles, creating the mesh with tetrahedral or hexahedral mesh cells will result in an excessively large cell number and loss of geometric features, reducing simulation accuracy and stability. To overcome this, the vortex generator domain is isolated from the liquid domain and connected to the liquid domain via the AMI interface [23]. The vortex generator domain is meshed with polyhedral elements using the Fluent mosaic meshing algorithm, and all geometric characteristics are captured with a high mesh quality with an averaged non-orthogonality of 1.8462. Fig. 1b shows the generated mesh for the vortex generator domain on a horizontal plane.

The first order, bounded, implicit Euler method is used as the time-marching scheme, the momentum term is discretized with the upwind Gauss linear method, the volume fraction term is discretized with the Gauss-vanLeer method, the gradient and divergence fields are discretized with Gauss linear method, and the Laplacian operator is discretized with the Gauss linear corrected method. The fluid is assumed to have the same working property as water, modeled as an incompressible Newtonian fluid with a density of 998.2 kg/m^3 and a viscosity of 0.001003 kg/m-s. The properties of the gas phase are assumed to be the same as air, an incompressible Newtonian fluid with a density of 1.22 kg/m^3 and a viscosity of 1.789×10^{-5} kg/m-s.

2.3. Boundary condition and scheme

Fig. 3 illustrates the boundary conditions for the raceway pond and a

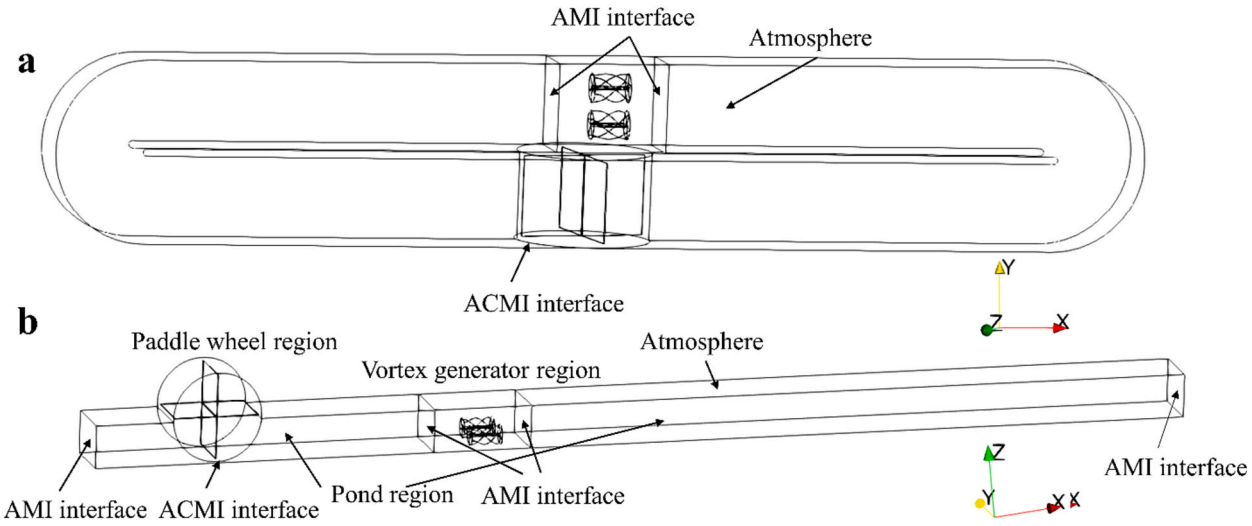

Fig. 3. (a) Boundary condition setup of the raceway pond simulation. (b) Boundary condition setup of the straight channel simulation.

straight channel with a vortex generator installed. Other than for the interface between the paddle wheel and pond regions, the top surface is configured as an ACMI boundary condition; the interface between the paddle wheel and pond regions is set as an atmosphere boundary condition. Other pond boundaries, such as the pond's wall, divider, and bottom, are specified to have no-slip wall boundary restrictions. Because the pond region and the vortex generator region are meshed differently, those two regions are connected by an AMI interface. For the straight channel simulation, the inlet and the outlet are paired with an AMI interface (Fig. 3b). The size of the time step is time-variant based on the Courant number, which is limited to 20 and the time step size is limited to 0.01 s.

2.4. Volume of fluid (VOF) model

The pond is modeled as a multiphase flow, and the volume of fluid (VOF) model is used to track the interface between the gas and liquid accurately and solve the flow field of both phases. Each microalgae cell's motion is assumed to have a negligible impact on liquid motion as well as fluid properties. The VOF model denotes each phase using a scalar function, the volume fraction α [24]. In our case: $\alpha = 0$ if the mesh cell is in the gas phase; $\alpha = 1$ if the mesh cell is in the liquid phase; and a value between 0 and 1 denotes that the mesh cell is at the interface. Density and viscosity are calculated as

$$\rho = \rho_g \alpha_g + \rho_l \alpha_l \tag{1}$$

$$\mu = \mu_g \alpha_g + \mu_l \alpha_l \tag{2}$$

where ρ is the density, μ is the viscosity, α is the volume fraction, and subscripts g and l denote the gas and liquid phases, respectively.

Considering the fluids modeled in raceway pond systems are incompressible, immiscible, and isothermal, the VOF model solves the continuity equation and the momentum equation:

$$\nabla \bullet \boldsymbol{u} = 0 \tag{3}$$

$$\frac{\partial}{\partial t}(\alpha_k \rho_k \boldsymbol{u}_k) = -\nabla \bullet ((\alpha_k \rho_k \boldsymbol{u}_k \boldsymbol{u}_k)) - \alpha_k \nabla p - \nabla \bullet (\alpha_k \overline{\boldsymbol{\tau}_k}) + \alpha_k \rho_k \boldsymbol{g} + \boldsymbol{F} \tag{4}$$

where p is the pressure, $\overline{\boldsymbol{\tau}}$ is the stress tensor, $\boldsymbol{g}$ is the gravity vector, $\boldsymbol{F}$ is the source term and subscript k denotes this equation is for the kth phase. The transport equation for the volume of fluid scalar α_k for the kth phase is:

$$\frac{\partial \alpha_k}{\partial t} + \nabla \bullet (\alpha_k \boldsymbol{u}_k) + \nabla \bullet (\alpha_k (1 - \alpha_k) \boldsymbol{u}_r) = 0 \tag{5}$$

where the third term is the artificial compression term and $\boldsymbol{u}_r$ is the artificial compressive velocity suitable to compress the interface [25,26].

2.5. Turbulence model

The large eddy simulation (LES) model is utilized as the turbulence model in order to get high-fidelity velocity fields for the analysis of the vortices' transient structures. The LES model employs a one-equation Smagorinsky-type eddy viscosity model created by Yoshizawa [27].

2.6. Determine persistence length using a critical vertical velocity

To determine the persistence length of the swirling motion generated by the paddle wheel in a raceway pond (Fig. 3a), as well as downstream of the vortex generators in the straight section (Fig. 3b), once the flow is fully developed at $t = 100$ s, the flow fields over a total of 15 s (from $t = 100$ s to $t = 115$ s), sampled at 0.2 s intervals are visualized and analyzed in Matlab. This includes a total of 75 velocity fields for each simulated case. The determination of the persistence length follows a procedure consisting of the following steps.

1. The velocity fields belonging to the air phase are excluded since the attributes of the velocity fields associated with the liquid phase are the primary focus for every velocity field frame.
2. The velocity fields' vertical component is evaluated against the critical velocity $u_{z,cri}$ for the remaining liquid portion. In cases where the vertical component is larger than the critical velocity at particular locations, those specific areas are retained, while other areas are discarded.
3. Since the horizontal distribution of swirling motion is of more interest than their vertical distribution, the liquid regions preserved from step 2 are projected onto a two-dimensional horizontal plane. This procedure is repeated for all 75 velocity fields in each scenario, and the retained liquid area that meets the condition of $\mathrm{abs}(u_z) > u_{z,cri}$ are overlapped to produce a map of the high vertical velocity regions. Those high vertical velocity regions, for example, are shown as black connected regions in Fig. 7.
4. The largest connected region is determined and enclosed by the red line, as shown in Fig. 7. The persistence length is measured from the outlet of the vortex generators, denoted by a vertical blue line in

Fig. 7, to the point where the connected regions occupy more than 30 % of the channel width at that location (denoted by a horizontal blue line).

To ensure accuracy in the persistence length calculation, the procedure is designed to take into account cases where the connected region contains a "thin tail" that might impact the calculation. In these cases, the fluid in these regions may exhibit some vertical motion, but the vertical motion is not strong enough to occupy enough volume for an accurate measurement. Including these areas in the persistence length calculation would result in an overestimation. Therefore, the 30 % criterion in step 4 excludes these regions from the persistence length calculation, which leads to a more accurate and precise calculation of persistence length.

3. Results and discussion

3.1. Flow field of a raceway pond with the vortex generators

Fig. 4a illustrates the contours of abs(u_z) in the horizontal plane midway between the interface and bottom when there are no vortex generators. It can be observed that high vertical velocity zones are formed downstream of the paddle wheel because of its motion, and downstream of the hairpin bends due to the secondary flow phenomena resulting from Dean flow. However, abs(u_z) is low compared to these high vertical velocity regions near the middle and the end portion of the second straight section as the swirling motion generated by the secondary flow dissipates. As shown in Fig. 4b, vortex generators are positioned in a counter directional configuration at the center of the second straight section, and abs(u_z) in the horizontal mid-plane is used to identify regions of high vertical velocity and swirling motion at a flow time point of 100 s. The swirling motion is weak upstream of the vortex generator entrances due to viscous dissipation. When fluid flows out a generator's exit, the swirling motion re-establishes and propagates downstream. It can be observed that the vortex generators successfully created two instances of swirling movements that propagated all the way to the second hairpin bend such that the abs(u_z) contour demonstrates four high vertical velocity traces. Fig. 4d illustrates the velocity magnitude contours in the horizontal mid-plane. It can be observed that the velocity magnitude of the flow downstream of the vortex generators is not impaired, indicating that adding the vortex generators in the straight channel does not increase the flow resistance significantly, and it does not increase the power consumption extensively.

3.2. Vortex generator deployment strategy

Since the five blades inside the vortex generator are curved in the same direction and the width of a raceway pond is invariably larger than the diameter of the generator, the generators must be situated in parallel and can be situated with blades oriented in the same direction or counter directional. Fig. 4b shows the abs(u_z) contour in the horizontal mid-plane when two vortex generators are placed in a counter direction. Compared to the unidirectional configuration (Fig. 4c), the swirling motion generated in the counter directional configuration occupies a larger volume and propagates for a longer distance. One explanation is that when multiple vortex generators are placed counter to one another, the downstream fluid flows in the same vertical direction at the center of two neighbor generators. To illustrate this, Fig. 5 displays the velocity fields in 3 vertical planes downstream of the vortex generators when they are oriented in a counter configuration, which is highlighted by the rotational direction of the internal blades. As the blades are curved clockwise in the right vortex generator and count clockwise in the left vortex, the swirling motion generated downstream of the vortex generators is oriented in the same direction as the blades. With the right swirling motion oriented clockwise and the left one oriented count clockwise, the fluid in the center flows uphill. On the contrary, when adjacent generators are placed with blades oriented in the same direction, the fluid between them will flow in opposite directions, with one

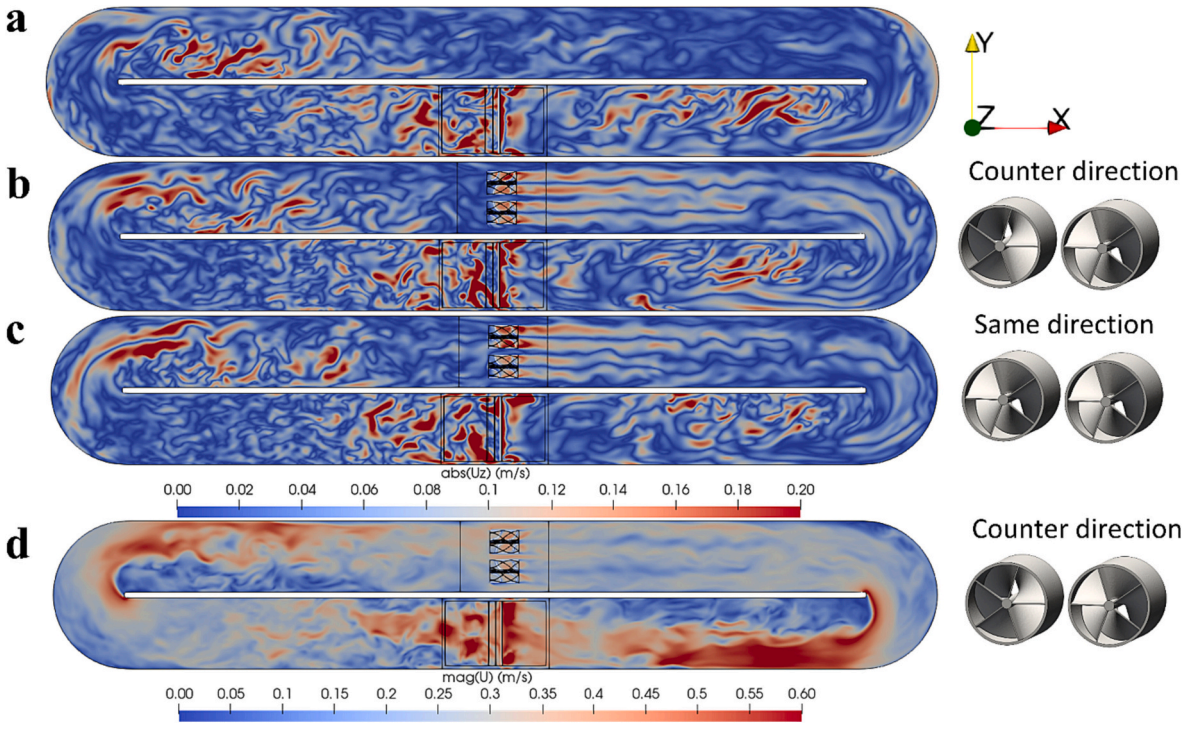

Fig. 4. (a) abs(u_z) contour at the horizontal plane at z = 0.1 m, flow time = 100 s where the vortex generators are not deployed. (b) abs(u_z) contour at the horizontal plane at z = 0.1 m, flow time = 100 s where the vortex generators are placed in counter directions. (c) abs(u_z) contour at the horizontal plane at z = 0.1 m, flow time = 100 s where the vortex generators are placed in the same directions. (d) mag($\boldsymbol{u}$) contour at the horizontal plane at z = 0.1 m, flow time = 100 s where the vortex generators are placed in counter directions.

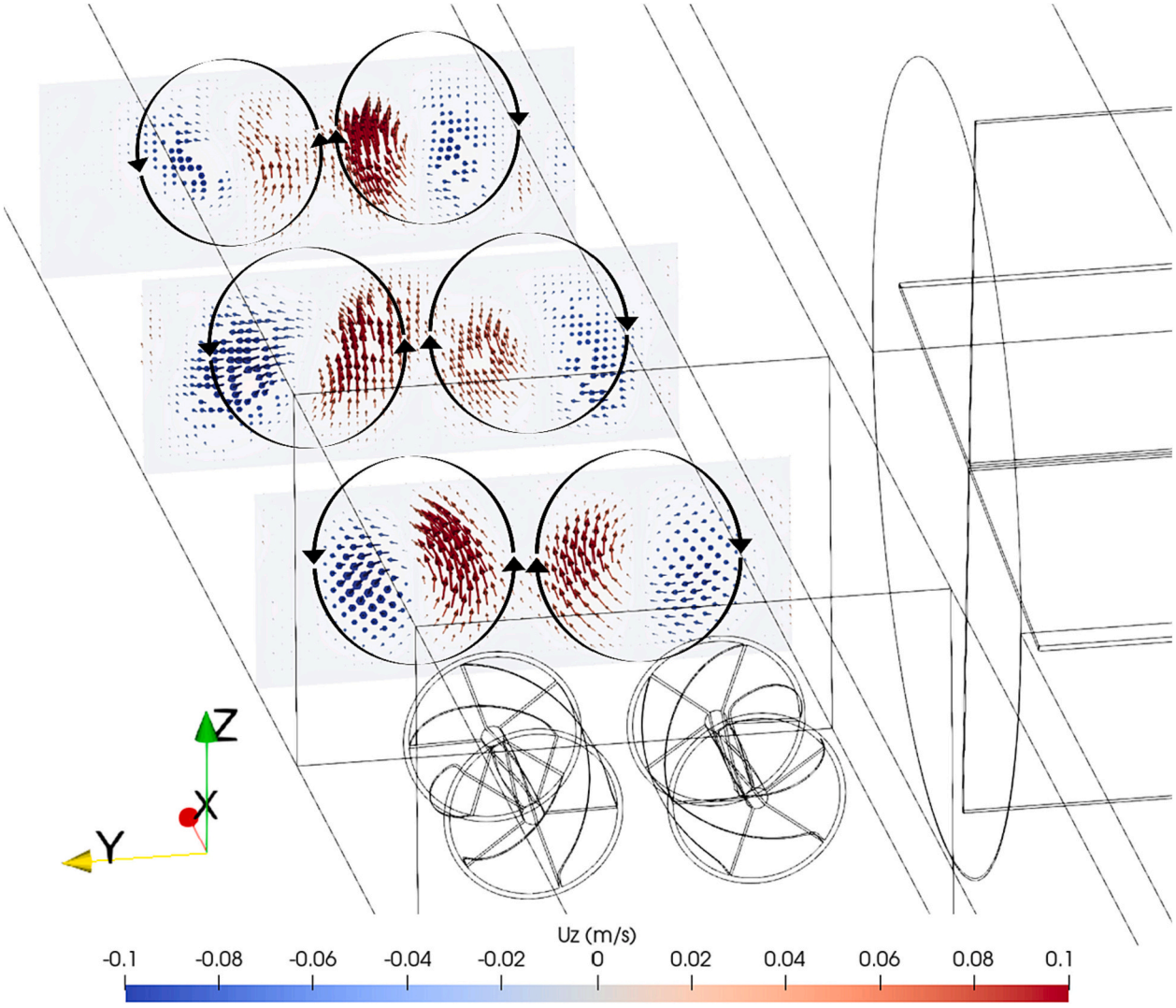

Fig. 5. Velocity fields on 3 vertical cross sections downstream the pair of vortex generators that is placed in the counter configuration. The velocity vectors are colored by the magnitude of $\boldsymbol{u_z}$.

flowing upward next to the other flowing downward, so that their momentum cancels to some extent, and as a result, the swirling motion cannot propagate as far as in the counter orientation due to this dampening effect.

3.3. Determine the optimal diameter of the vortex generator

It is hypothesized that there exists an optimal generator diameter is relative to the water depth of the raceway pond. If the diameter of the generator exceeds the liquid depth of the pond, a portion of the generator will protrude through the air-liquid interface, preventing the liquid from turning completely inside the generator. When the diameter of the generator is significantly smaller than the water depth, it is hypothesized that the swirling motion generated will have a reduced strength and dissipate faster as liquid flows over the top of the generator.

To address these hypotheses and determine the optimal diameter for a vortex generator, three water depths were simulated (0.1, 0.15, and 0.25 m), rather than changing the diameter of the generators and placing them in a constant water depth. As it was determined in Section 3.2 that placing the vortex generators in a counter configuration results in a stronger swirling motion with a longer persistence length, the vortex generators are configured this way to investigate the optimal diameter in this part of the study. Fig. 6a displays the contours of abs(u_z) in the horizontal mid-plane ($z = 0.05$ m) for a water depth of 0.1 m. When the water depth is set to 0.1 m, the generators are unable to produce a significant swirling motion, with 44 % of the generator body protruding through the air-water interface. However, vortices can still be observed downstream of the vortex generators, albeit at a much weaker strength than the swirling motion depicted in Fig. 4b.

When the water depth is set to 0.15 m, slightly less than the diameter of the vortex generator, the resulting abs(u_z) contours in the horizontal mid-plane ($z = 0.075$ m) can be seen in Fig. 6b. It reveals that the swirling motion generated is sufficiently strong to be observed in the abs (u_z) contours and is significantly stronger than the case with the 0.1 m water depth. Although the liquid cannot make a full turn inside the generators due to the section of the generators protruding through the liquid-gas interface, significant swirling motions can be observed downstream of the generators.

For the 0.25 m water depth, Fig. 6c displays the abs(u_z) contours at the horizontal mid-plane ($z = 0.125$ m). The swirling motion downstream of the generators has a comparable strength as in the 0.15 m water depth case.

In none of these cases does the generated swirling motion persist as far as the 0.2 m water depth scenario shown in Fig. 4b. As there is considerable liquid flowing above the vortex generators when liquid depth is 0.25 m, that liquid is primarily flowing horizontally, and has the

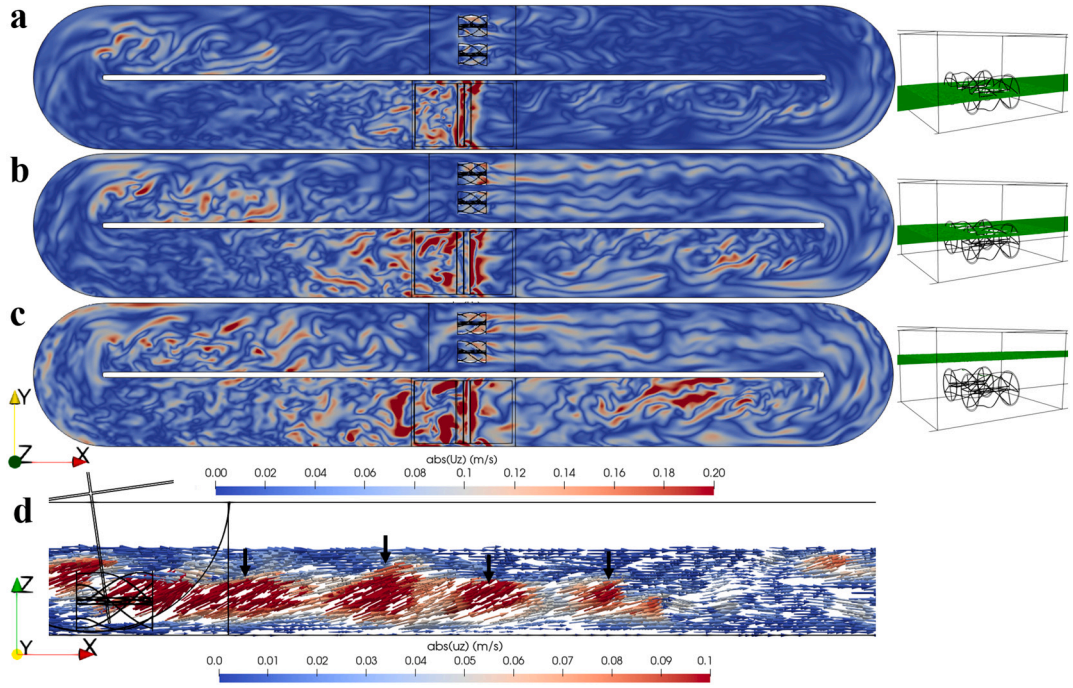

Fig. 6. (a) abs(u_z) contour at the horizontal plane at z = 0.1 m, flow time = 100 s, vortex generator diameter = 0.16 m, water depth = 0.1 m. Vortex generators are placed in counter directions. (b) abs(u_z) contour at the horizontal plane at z = 0.1 m, flow time = 100 s, vortex generator diameter = 0.16 m, water depth = 0.15 m. Vortex generators are placed in counter directions. (c) abs(u_z) contour at the horizontal plane at z = 0.15 m, flow time = 100 s, vortex generator diameter = 0.16 m, water depth = 0.25 m. Vortex generators are placed in counter directions. (d) velocity field at a vertical plane downstream of the vortex generator, flow time = 100 s, vortex generator diameter = 0.16 m, water depth = 0.25 m.

potential to interfere with the swirling motion downstream of the generators. This potential interference is demonstrated in Fig. 6d, where the velocity field of a vertical cross section is plotted and colored by abs(u_z). It can be observed that there is considerable liquid above the swirling motion that flows horizontally from the left to the right of the section, and the positions where the high vertical velocity region contacts with the horizontal flow are marked with black arrows. It is logical to assume that when those two flows are in contact, their momentum will be exchanged, and as the result, the swirling motion is negatively impacted, and the persistence length is reduced in comparison to the 0.2 m water depth case (Fig. 4b).

By studying the abs(u_z) contours in the horizontal plane located at the center of the liquid region at various operating water depths, there is the somewhat obvious conclusion that the diameter of the vortex generators should be equal to or slightly smaller than the operating water depth. If the diameter of the generator is greater than the water depth, the liquid cannot make complete rotations inside the generators, and the angular momentum cannot be sustained for a long distance downstream of the generators. When the generator diameter is significantly less than the liquid depth (more than 3 cm smaller), the fluid flow above the generators may interfere with the swirling motion generated downstream of the generators and have a negative impact on the persistence length of the generated swirling motion. It is important to note that there is some leeway in the relationship between generator diameter and water depth. The generator can protrude 15 % above the interface or lie 25 % below the interface and still produce a significant swirling flow that persists for long distances.

3.4. Determine the optimal length

To determine the optimal length L_{opt}, vortex generators with the lengths of 0.1, 0.15, 0.2, 0.25, 0.3, and 0.4 m with the same blade pitch are implemented in a straight channel where the fluid is driven by a paddle wheel. The external diameters of all the vortex generators are 0.18 m, and the water depth is 0.2 m.

A straight channel is utilized to eliminate the secondary flow effect created by the bends, and the straight channel's inlet and outlet are coupled to AMI boundary conditions to impose periodic boundary conditions where the same flow field information will be distributed. Thus, the swirling motion caused by the hairpin is avoided, and the swirling motion caused by vortex generators of various designs can be isolated and compared at a reduced computational cost.

The performance of the vortex generators can be characterized by the volume fraction of liquid containing the high vertical velocity regions downstream of the generators, with a larger occupied volume and a longer persistence length indicating better performance. As illustrated in Fig. 4b, and c, the high vertical velocity zones occupy the majority of the space across the channel width in all circumstances. Thus, rather than calculating the volume of liquid occupied by the high vertical velocity regions, the persistence length of these regions is utilized to quantify the vortex generators' performance. Section 2.6 covers the procedure for calculating the persistence length for various critical vertical velocity magnitudes, with measurements starting from the outlet of the vortex generators.

The persistence lengths for the six different generator lengths are presented in Fig. 7, with the outlet of each vortex generator marked by a vertical blue line and the computed persistence length denoted by a horizontal blue line. It can be observed that when the critical vertical velocity magnitude increases, the persistence length for all the cases decreases, which is reasonable as a more liquid region is filtered out when a larger critical vertical velocity is used, resulting in a shorter persistence length.

When 0.12 m/s is used as the critical vertical velocity, the persistence length decreases from 3.90 m to 3.73 m when the vortex generator length increases from 0.1 m to 0.15 m and then continues to increase up to a generator length of 0.3 m. A significant persistence length decrease can be observed when the length of the vortex generator increases from 0.3 m to 0.4 m. When the length is between 0.1 m and 0.3 m, the fluid

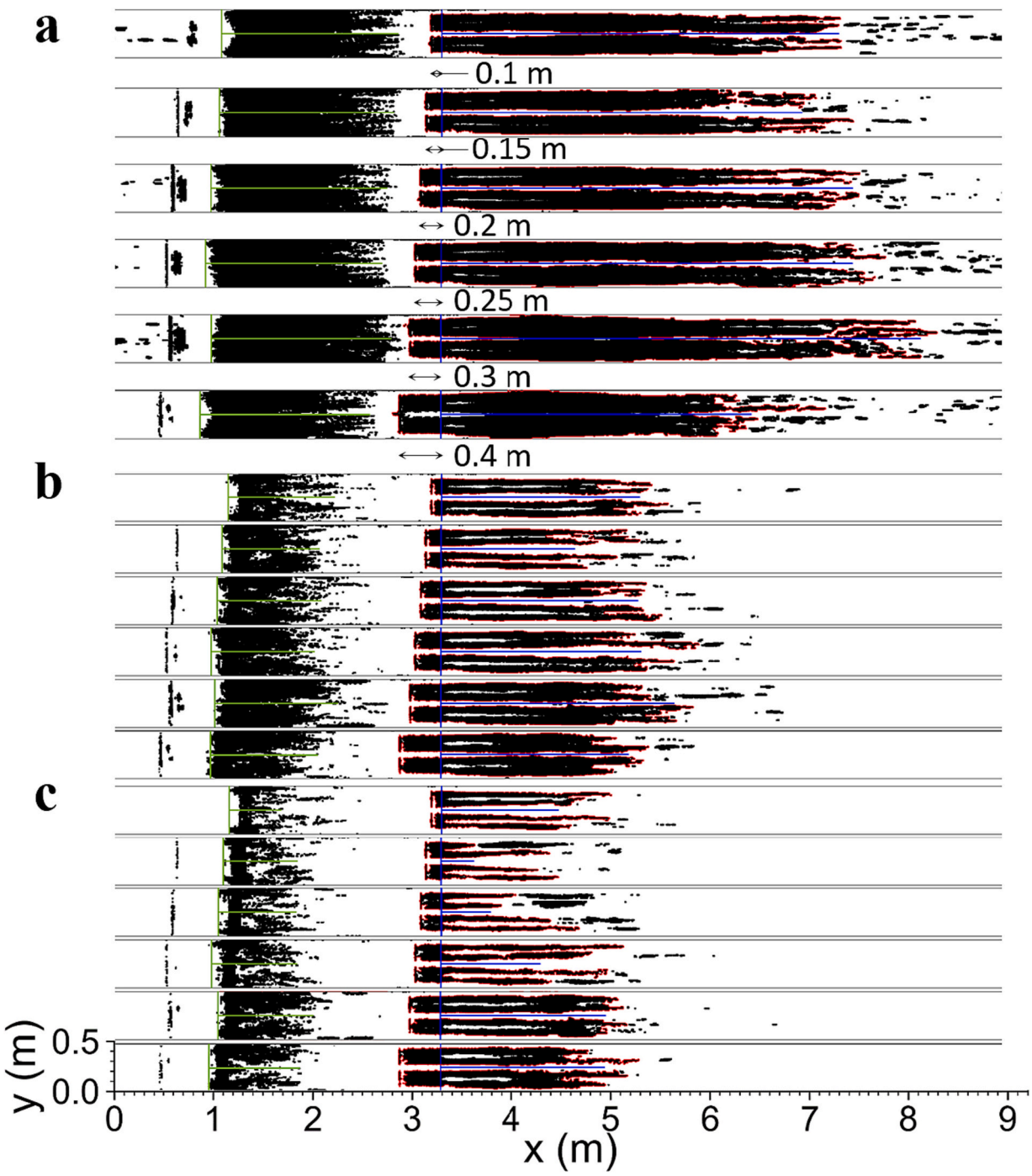

Fig. 7. High vertical velocity regions and persistence length of swirling motion generated by the paddle wheel (horizontal green line) and swirling motion generated by vortex generators (horizontal blue line) (a) Critical vertical velocity = 0.12 m/s. (b) Critical vertical velocity = 0.16 m/s. (c) Critical vertical velocity = 0.18 m/s. (For interpretation of the references to colour in this figure legend, the reader is referred to the web version of this article.)

spends more time inside the generators and gains more angular momentum and therefore, results in a longer persistence length. However, when the length is further increased above 0.3 m, it is believed that the resistance force that fluid experienced due to the internal propeller blades is increased to the point that the performance of the 0.4 m long vortex generator deteriorates. Similar results can be observed when the critical vertical velocities are set to 0.16 and 0.18 m/s.

The longest persistence lengths of 2.25 m and 1.67 m are obtained when the generators are 0.3 m in length, which can be explained by the extra angular momentum gained by the fluid with a longer generator length. Thus, when the critical vertical velocity is between 0.16 and 0.18 m/s, the optimal length is 0.3 m.

When the generator's length is increased above 0.3 m, the persistence length decreases and the performance to generate whirling motion deteriorates. When the critical vertical velocity is set to 0.18 m/s, the retained high velocity region is the core of the swirling motion where the rotational speed is high and occupies a considerably smaller volume compared to the case with a lower critical vertical velocity such as 0.12 m/s (Fig. 7a and c). However, the volume of high vertical velocity regions within the vortex generators is comparable, indicating that the fluid gains significant angular momentum almost as soon as it enters the inlets of the vortex generators. When the length of the generator is

increased from 0.1 m to 0.15 m, the resulting persistence length is decreased. One possible explanation for this is that the shorter length in the 0.1 m length scenario imposes a less resistance force for the fluid and therefore, a longer persistence length can be achieved. Regardless, observation was consistent regardless of the specifics of how persistence length is calculated.

To summarize, when the swirling motion persistence length is considered along with three crucial vertical velocities, the L_{opt} is determined to be 0.3 m. At this length:diameter ratio, the generated swirling motion occupies the largest volume downstream of the generator (shown in Fig. 7a and b), with the core of the swirling motion persisting the longest distance (Fig. 7c).

However, when the material costs are taken into consideration, the 0.1 m long vortex generator achieves an impressive degree of swirling motion where the averaged persistence length is 81.8 % of the best case when $u_{z,cri} = 0.18$ m/s and the persistence length is only 25.8 % lower than the 0.3 m generator when 0.12 m/s is chosen as the critical vertical velocity. When a higher critical vertical velocity is used, the persistence length of the 0.1 m system still shows a long persistence length close to the 0.30 m long design. For ponds with extremely long straight sections, it may be more cost effective to install multiple instances of the 0.1 m generators.

3.5. Swirling motion morphology

A significant finding from this work is that the vertical motion induced by the paddle wheel's rotational motion cannot propagate over a significant distance, as illustrated in Figs. 4 and 7. The region of high vertical velocity observed using three distinct critical vertical velocities reveals that the swirling motion generated by the paddle wheel has a substantially shorter persistence length than the swirling motion downstream of the vortex generators (Fig. 8). When $u_{z,cri} = 0.12$ m/s is utilized, the persistence length of the swirling motion generated by the paddle wheel is estimated to be 1.75 m, whereas the swirling motion generated by the 0.1 m long vortex generator can continue up to 3.90 m. This is also the case when a critical vertical velocity of 0.18 m/s is employed. The swirling motion generated by the paddle wheel is limited to 0.77 m, whereas the 0.1 m long vortex generator can induce swirling motion that can propagate as far as 1.28 m. As the length:radius ratio of a commercial raceway pond, such as the RW101 raceway pond design developed by MicroBio Engineering Inc., can easily reach 20, it is believed that vertical mixing induced by the paddle wheel is limited and the swirling motion generated by the paddle wheel can only persist for a short distance. This inadequacy can be explained by the morphology of the swirling motion. Fig. 9 represents the isosurface for a Q criterion of 5. When the swirling motion is generated by the rotational motion of the paddle wheel, the rotational axis of the swirling motion is perpendicular to the direction of the main flow.

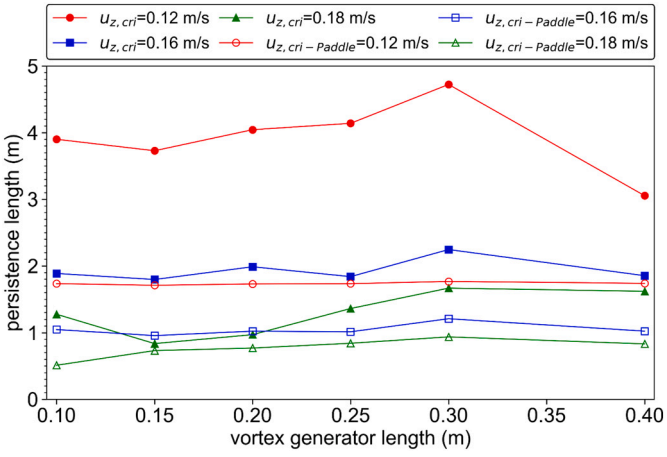

Fig. 8. Persistence length of the swirling motion generated by the vortex generators and the paddle wheel.

Since the fluid velocity field is not uniform along the direction of the y-axis, the swirling motion transported downstream the paddle wheel breaks up into smaller vortexes, and their axes are turned to the direction of the main flow, which is illustrated in Fig. 9. On the contrary, the rotational axis of the swirling motion generated by the secondary flow downstream the hairpin bend as well as the ones downstream the vortex generators are parallel to the direction of the primary flow. The results of the straight channel simulation (Figs. 7 and 8), as well as the one with the raceway pond geometry (Fig. 4a, b, and c) suggest that the swirling motion does not dissipate as quickly when the axis is parallel to the main flow direction, and therefore, can persist for a longer distance. Since the swirling motion induced by the vortex generators has a similar morphology to the one generated by the secondary flow, it is believed that the swirling motion generated by the hairpin bend also benefits from this mechanism.

4. Conclusion

In this study, the novel design and investigation of a vortex generator with inclined internal baffles is presented. Its performance to enhance vertical motion by generating vortices downstream of the generator is evaluated and quantified using CFD simulations in which the vortex generator is located in the second straight section of a raceway, as well as in a straight channel with a paddle wheel. The CFD results indicate the following:

1. It is predicted that there is a significant enhancement of vertical mixing downstream of the vortex generator.
2. To obtain optimal vertical mixing and persistence length, the vortex generator pairs should be placed with blades oriented in a counter configuration such the fluid motion is symmetrical between two adjacent generators, and the vertical motion is enhanced as a result.
3. The generator's diameter should be slightly smaller than the intended water depth. For example, for a pond with a 0.2 m depth, the optimal diameter appears to be around 0.18 m. If the generator's diameter is significantly larger than the water depth, the fluid cannot make complete turns inside the vortex generator, and the swirling motion cannot persist reasonably far. Leaving excessive space above the vortex generator is also considered sub-optimal since the horizontal flow above tends to dampen the generated swirling motion.
4. The optimal length is determined to be around 0.3 m for a 0.18 m-diameter vortex generator. However, it is found that a vortex generator with a length of 0.1 m can still generate significant secondary motion such that the persistence length will be only 18.2 % less than the optimal scenario and may be desirable when the material costs are taken into account.
5. The paddle wheel is thought to have a significant impact on the mixing performance in raceway pond systems. However, the results of the straight channel simulations suggest that the swirling motion generated by a paddle wheel cannot persist over a distance comparable to the swirling motion generated downstream of the current vortex generator design. Since the swirling motion induced by the paddle wheel has an axis that is perpendicular to the direction of the main flow, the eddies are broken up into smaller, weaker vortices. Therefore, one strategy identified in this study is to induce swirling motion with a rotational axis parallel to the main flow direction in order to obtain optimal vertical mixing enhancement.

Author statement

The authors confirm thier contribution to the paper as follows: study conception and design: Chen Shen, David Dandy; data collection: Chen Shen; analysis and interpretation of results: Chen Shen; Original Draft: Chen Shen; Review & Editing: David Dandy; Supervision: David Dandy;

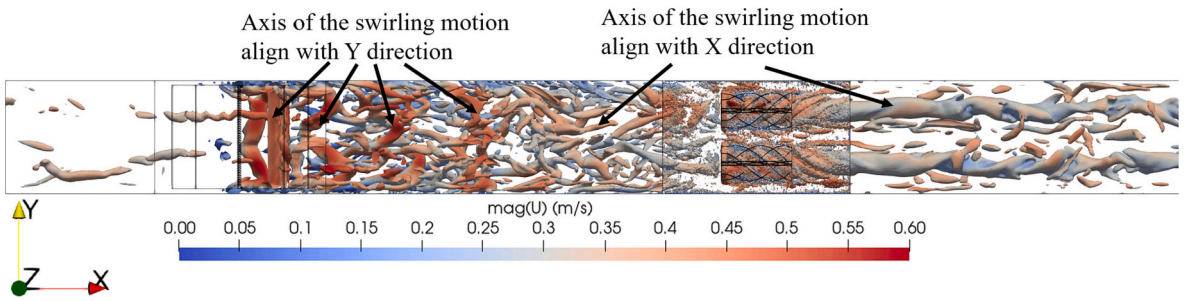

Fig. 9. Iso-surfaces Q-criterion = 5 at flow time = 100 s where 0.3 m long vortex generators are placed in counter directions in a straight channel.

All authors reviewed the results and approved the final version of the manuscript.

CRediT authorship contribution statement

Chen Shen: Conceptualization, Data curation, Formal analysis, Investigation, Methodology, Software, Validation, Visualization, Writing – original draft. **David S. Dandy:** Conceptualization, Funding acquisition, Methodology, Project administration, Supervision, Writing – review & editing.

Declaration of competing interest

The authors declare that they have no known competing financial interests or personal relationships that could have appeared to influence the work reported in this paper.

Data availability

Data will be made available on request.

Acknowledgments

This work was supported by NSF award no. 1332404 and DOE award no. DE-EE00-08514. We thank the National Renewable Energy Laboratory for providing access to their high-performance computing resources.

References

[1] J.E. Keffer, G.T. Kleinheinz, Use of *Chlorella vulgaris* for CO2 mitigation in a photobioreactor, J. Ind. Microbiol. Biotechnol. 29 (5) (Nov. 2002) 275–280, https://doi.org/10.1038/sj.jim.7000313.

[2] A.P. Carvalho, S.O. Silva, J.M. Baptista, F.X. Malcata, Light requirements in microalgal photobioreactors: an overview of biophotonic aspects, Appl. Microbiol. Biotechnol. 89 (5) (Mar. 2011) 1275–1288, https://doi.org/10.1007/s00253-010-3047-8.

[3] "A matter of detail: Assessing the true potential of microalgal biofuels-Klein-Marcus- chamer - 2013 - Biotechnology and Bioengineering - Wiley Online Library." https://onlinelibrary.wiley.com/doi/full/10.1002/bit.24967 (accessed Oct. 04, 2021).

[4] C. Posten, Design principles of photo-bioreactors for cultivation of microalgae, Eng. Life Sci. 9 (Jun. 2009) 165–177, https://doi.org/10.1002/elsc.200900003.

[5] F.G. Acién, et al., 1 - Photobioreactors for the production of microalgae, in: C. Gonzalez-Fernandez, R. Muñoz (Eds.), Microalgae-Based Biofuels and Bioproducts, Woodhead Publishing, 2017, pp. 1–44, https://doi.org/10.1016/B978-0-08-101023-5.00001-7.

[6] C. Jiménez, B.R. Cossío, D. Labella, F. Xavier Niell, The feasibility of industrial production of Spirulina (Arthrospira) in Southern Spain, Aquaculture 217 (1) (Mar. 2003) 179–190, https://doi.org/10.1016/S0044-8486(02)00118-7.

[7] "Microalgae for oil: Strain selection, induction of lipid synthesis and outdoor mass cultivation in a low-cost photobioreactor - Rodolfi - 2009 - Biotechnology and Bioengineering - Wiley Online Library." https://onlinelibrary.wiley.com/doi/abs/10.1002/bit.22033 (accessed Oct. 04, 2021).

[8] O. Jorquera, A. Kiperstok, E.A. Sales, M. Embiruçu, M.L. Ghirardi, Comparative energy life-cycle analyses of microalgal biomass production in open ponds and photobioreactors, Bioresour. Technol. 101 (4) (Feb. 2010) 1406–1413, https://doi.org/10.1016/j.biortech.2009.09.038.

[9] S. Abu-Ghosh, D. Fixler, Z. Dubinsky, D. Iluz, Flashing light in microalgae biotechnology, Bioresour. Technol. 203 (Mar. 2016) 357–363, https://doi.org/10.1016/j.biortech.2015.12.057.

[10] Z. Chen, X. Zhang, Z. Jiang, X. Chen, H. He, X. Zhang, Light/dark cycle of microalgae cells in raceway ponds: effects of paddlewheel rotational speeds and baffles installation, Bioresour. Technol. 219 (Nov. 2016) 387–391, https://doi.org/10.1016/j. biortech.2016.07.108.

[11] K. Lee, C.-G. Lee, Effect of light/dark cycles on wastewater treatments by microalgae, Biotechnol. Bioprocess Eng. 6 (3) (Jun. 2001) 194–199, https://doi.org/10.1007/BF02932550.

[12] G. Persoone, J. Morales, H. Verlet, and N. De Pauw, "Air-lift pumps and the effect of mixing on algal growth," 2000. Accessed: Oct. 04, 2021. [Online]. Available: http://www.vliz.be/imisdocs/publications/128033.pdf.

[13] "Biological Principles of Mass Cultivation of Photoautotrophic Microalgae - Handbook of Microalgal Culture - Wiley Online Library." https://onlinelibrary.wiley.com/doi/abs/10.1002/9781118567166.ch11 (accessed Oct. 04, 2021).

[14] "Large-Scale Production of Algal Biomass: Raceway Ponds | SpringerLink." https://link.springer.com/chapter/10.1007/978-3-319-12334-9_2 (accessed Oct. 04, 2021).

[15] J.P. Bitog, et al., Application of computational fluid dynamics for modeling and designing photobioreactors for microalgae production: a review, Comput. Electron. Agric. 76 (2) (May 2011) 131–147, https://doi.org/10.1016/j.compag.2011.01.015.

[16] J.C.M. Pires, M.C.M. Alvim-Ferraz, F.G. Martins, Photobioreactor design for microalgae production through computational fluid dynamics: a review, Renew. Sustain. Energy Rev. 79 (Nov. 2017) 248–254, https://doi.org/10.1016/j.rser.2017.05.064.

[17] "Light-field-characterization in a continuous hydrogen-producing photobioreactor by optical simulation and computational fluid dynamics - Krujatz - 2015 - Biotechnology and Bioengineering - Wiley Online Library." https://onlinelibrary.wiley.com/doi/full/10.1002/bit.25667 (accessed Oct. 04, 2021).

[18] L. Wang, Y. Tao, X. Mao, A novel flat plate algal bioreactor with horizontal baffles: structural optimization and cultivation performance, Bioresour. Technol. 164 (Jul. 2014) 20–27, https://doi.org/10.1016/j.biortech.2014.04.100.

[19] R.S. Voleti, Experimental Studies of Vertical Mixing in an Open Channel Raceway for Algae Biofuel Production, 2012.

[20] Z. Yang, J. Cheng, Q. Ye, J. Liu, J. Zhou, K. Cen, Decrease in light/dark cycle of microalgal cells with computational fluid dynamics simulation to improve microalgal growth in a raceway pond, Bioresour. Technol. 220 (Nov. 2016) 352–359, https://doi.org/10.1016/j.biortech.2016.08.094.

[21] Q. Zhang, S. Xue, C. Yan, X. Wu, S. Wen, W. Cong, Installation of flow deflectors and wing baffles to reduce dead zone and enhance flashing light effect in an open raceway pond, Bioresour. Technol. 198 (Dec. 2015) 150–156, https://doi.org/10.1016/j.biortech.2015.08.144.

[22] H.G. Weller, G. Tabor, H. Jasak, C. Fureby, A tensorial approach to computational continuum mechanics using object-oriented techniques, Comput. Phys. 12 (6) (Nov. 1998) 620–631, https://doi.org/10.1063/1.168744.

[23] P.E. Farrell, J.R. Maddison, Conservative interpolation between volume meshes by local Galerkin projection, Comput. Methods Appl. Mech. Eng. 200 (1–4) (2011) 89–100.

[24] C.W. Hirt, B.D. Nichols, Volume of fluid (VOF) method for the dynamics of free boundaries, J. Comput. Phys. 39 (1) (Jan. 1981) 201–225, https://doi.org/10.1016/0021-9991(81)90145-5.

[25] B.E. Larsen, D.R. Fuhrman, J. Roenby, Performance of interFoam on the simulation of progressive waves, Coast. Eng. J. 61 (3) (Jul. 2019) 380–400, https://doi.org/10.1080/21664250.2019.1609713.

[26] D. J. Piro and K. J. Maki, "An adaptive interface compression method for water entry and exit," Mar. 2013, Accessed: Oct. 05, 2021. [Online]. Available: http://deepblue.lib.umich.edu/handle/2027.42/97021.

[27] A. Yoshizawa, Statistical theory for compressible turbulent shear flows, with the application to subgrid modeling, Phys. Fluids 29 (7) (Jul. 1986) 2152–2164, https://doi.org/10.1063/1.865552.